Journal of Alloys and Compounds 817 (2020) 153327

Contents lists available at ScienceDirect

Journal of Alloys and Compounds

journal homepage: http://www.elsevier.com/locate/jalcom

Diffusion assisted interaction of shear bands in metallic glasses

Zsolt Kovács*, Ádám Révész, Mohammed Ezzeldien [1], János Lendvai

Dept. of Materials Physics, Eötvös Loránd University, H-1117, Pázmány P. st. 1/a, Budapest, Hungary

ARTICLE INFO

Article history:
Received 30 September 2019
Received in revised form
6 December 2019
Accepted 7 December 2019
Available online 10 December 2019

Keywords:
Metallic glass
Plasticity
Shear band
Diffusion

ABSTRACT

Shear bands were formed at room temperature in $Zr_{44}Ti_{11}Cu_{10}Ni_{10}Be_{25}$ bulk metallic glass subjected to torsional deformation. Shear offset distribution was determined quantitatively for intersecting bands and compared to an elastic continuum shear defect model applied to similar band arrangements. The model reproduced the measured offset distribution, the residual stress field and different asymmetrical features of the band interaction. Differences between the model and the experimental results revealed the presence of a diffusion process for dilatational defects in shear band interaction.

1. Introduction

Glasses are mostly transparent and brittle materials with covalent bonds. In the 1960s, Duwez et al. demonstrated that metallic alloys can also be quenched into glassy structure [1]. While covalent glasses break under stress with conchoidal fracture through the formation of dangling bonds, metallic glasses generate shear bands along which they remain macroscopically cohesive. This fracture tolerant behavior of metallic glasses [2,3] opened up new possibilities in special structural applications [4,5] and focused scientific research on the macroscopic plasticity [6,7] and atomic scale evolution of shear bands [8–11].

Metallic glasses have attractive features as structural materials, such as high strength and large elastic limit [4,5]. On the other hand, they posses poor performance due to the localization of plastic deformation when deformation should be tolerated at low temperatures. At ambient conditions, fracture occurs in uniaxial tests along a shear band (SB) with extreme large local shear strains but tiny macroscopic plastic deformation [5]. The SBs are thin (~10–20 nm) two dimensional features, which concentrate plastic deformation to a fraction of the stressed material [12,13]. Despite this strong strain localization, high critical stress intensity factors were measured in different bulk metallic glasses [2,3], which focused scientific research to the peculiarity of formation and multiplication of SBs [7].

Disordered materials usually exhibit localized microscopic shear events under stress. These events in metallic glasses occur in shear transformation zones (STZs) [14] which form due to the high variability of the local atomic order for metallic bounds [15]. Yet, SB formation based on STZs is not fully understood [6,7], multi stage scenarios have been proposed [7,16,17]. Simulation of STZ dynamics revealed that the early stage of shear localization includes STZ clustering followed by nucleation and thickening of the SB [8]; meanwhile irreversible changes occur in the glassy structure by disintegration of dense icosahedral atomic environments and agglomeration of looser “liquid-like” units in the SB plane [9,11]. At the onset of plastic deformation, therefore, SBs undergo rapid softening and sudden plastic strain localization in metallic glasses. These unstable deformation modes are often uncontrolled and lead to the abrupt failure of the material during uniaxial tests. However, shear bands can be generated in a controlled way, e.g. in torsion deformation, due to the stress gradient developing along the sample radius and large plastic strains can be achieved in free-end torsion tests [18,19].

Shear band formation induces structural changes in the glass, such as the appearance of microscopic voids [20], complex long-range softening near the band trajectory [21] and residual stresses with normal and shear components with highly dipole character, extending over several micrometer from the band [22,23]. Quantitative evaluation of the stress field around SBs is only feasible in glasses, if a proper frame of reference is defined

* Corresponding author.
E-mail address: kovacszs@metal.elte.hu (Z. Kovács).
[1] Present address for M. Ezzeldien: Metallurgy and Material Science Tests Laboratory, Department of Physics, Faculty of Science, South Valley University, Egypt.

https://doi.org/10.1016/j.jallcom.2019.153327

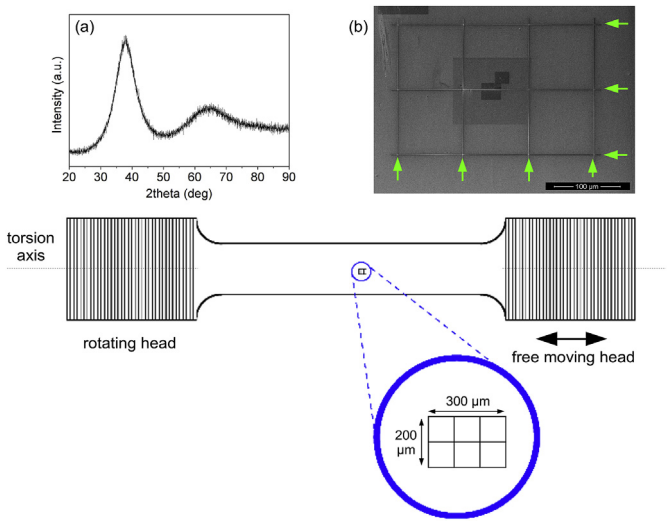

Fig. 1. Schematic image of the free-end torsion sample with a fine, focus ion beam milled marker grid on the surface. Enlarged view shows the dimensions of the marker. Inset (a) displays the X-ray diffraction pattern of the fully amorphous as-cast alloy of the samples and inset (b) is a SEM image exhibits the realized FIB milled marker lines indicated by green arrows. (For interpretation of the references to color in this figure legend, the reader is referred to the Web version of this article.)

[23]. For instance, a marker grid can be ion milled into the sample surface and changes of the grid can be analyzed after deformation in a similar way as it was performed in crystalline [24] and also glassy [25] disks which were then subjected to shear deformation in high pressure torsion.

In this paper, similarly, a marker grid was ion milled into the surface of each bulk metallic glass sample and displacements due to the formed shear bands were characterized quantitatively. Interaction between two intersecting bands was observed in the area defined by the markers, and based on the determined shear offset distributions interaction of the shear bands was analyzed in detail.

2. Experimental methods

An as-cast rod-shape bulk metallic glass alloy with composition of $Zr_{44}Ti_{11}Cu_{10}Ni_{10}Be_{25}$ (Vitreloy1b, Liquid metal Technologies, Inc., USA) was used in the present investigations. Amorphous behavior and incidental crystalline content of the as-cast alloy were checked by X-ray diffraction (see inset (a) in Fig. 1). These results characterized the as-cast alloy as a fully amorphous bulk metallic glass alloy.

For deformation experiments, cylindrical samples were machined from the as-cast glass (with L = 10 mm gauge length and R = 1 mm radius) joining to sample heads at both ends. Free-end torsion tests were performed on a torsion machine in which the twisted sample can freely contract or elongate and the stress state approaches a simple shear in the sample. We have performed a large batch of deformation tests, and two specimens have been selected for further, more detailed analysis. Before deformation, the surface of these samples has been carefully polished by alumina suspension down to 50 nm particle size. Thereafter, fine marker lines in a 200 μm × 300 μm grid with 100 μm spacing were milled onto the cylindrical surface of the specimens by a focused ion beam (FIB) of 30 kV Ga ions in a dual beam FEI Quanta 3D scanning electron microscope (see the schematic image in Fig. 1 and the realized pattern in the inset (b) of Fig. 1). The width of these grid lines was about 300 nm coupled with ~300 nm deep trenches along the lines. Subsequently, the two samples have been deformed in the torsion machine at ambient condition up to $\theta = 0.45$ rad and $\theta = 0.65$ rad rotation angles and then unloaded to M = 0 Nm torque at the same constant 0.005 rad/s rotation rate.

Imaging of the cylindrical surface of samples has been performed in the same dual beam FEI Quanta 3D scanning electron microscope (SEM) by 30 keV electrons using an ETD detector. Atomic force microscopy (AFM) was also applied to image surface features on the deformed torsion samples and measure radial offsets along shear bands using a AIST-NT Smart SPM-1000 equipment in non-contact mode.

3. Results

Torsion experiments performed on the two Vitreloy 1b bulk metallic glass samples exhibit good repeatability, but different plastic deformation as seen in the torque vs. rotation curves shown in Fig. 2a. The corresponding average surface shear stress vs. surface shear strain curves (see Fig. 2b) were calculated as $\tau(\gamma) = \frac{1}{2\pi R^3}\left(3M + \frac{dM}{d\theta}\theta\right)$, where the surface strain is determined as $\gamma = \frac{R\theta}{L}$ from the rotation angle. As seen, yield occurs at $M \approx 1.3$ Nm torque which corresponds to about $\tau = \tau_{max} = 1GPa$ yield stress at about $\gamma = 0.035$ shear strain. At larger shear deformations, the shear stress levels off, while the torque reaches different maximum

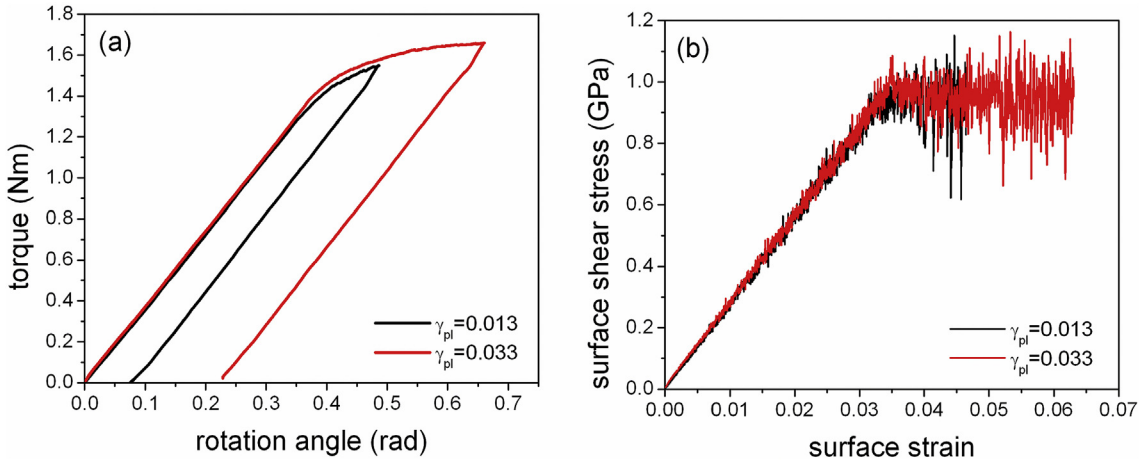

Fig. 2. (a) Experimental torque rotation angle curves obtained in load unload cycle of free-end torsion tests in $Zr_{44}Ti_{11}Cu_{10}Ni_{10}Be_{25}$ BMG. (b) surface stress vs. surface strain curves calculated from the torque rotation angle curves.

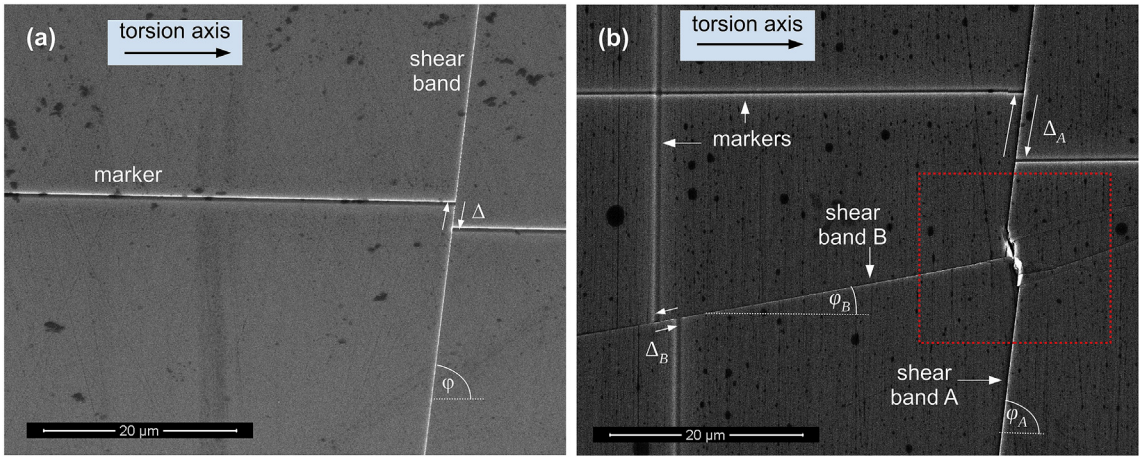

Fig. 3. Scanning electron microscopy images of the surface of torsionally deformed Vitreloy 1b bulk metallic glass samples with (a) $\gamma_{pl} = 0.013$ and (b) $\gamma_{pl} = 0.033$ plastic surface shear strain. Fine lines of the shear bands and the markers are indicated. Δ shear offset for $\gamma_{pl} = 0.013$ and Δ_A and Δ_B shear offsets for $\gamma_{pl} = 0.033$ are clearly visible at the markers.

values for the two tests at about $M = 1.6$ Nm and $M = 1.7$ Nm, respectively, due to the different plastic volumes. Following the unloading stage of the deformation sequence, the residual torsional deformation, θ_{pl}, is about 0.08 rad and 0.023 rad, which accounts for a respective average plastic shear strain $\gamma_{pl} = 0.013$ and 0.033 at the surface (see Fig. 2b). Due to the constraints of the elastic core and the heads of the sample in torsion, this plastic deformation can realize as multiple shear bands in the metallic glass samples (see Section 8.1 in Ref. [26]).

These shear bands develop during plastic deformation as sharp lines compared to the wider markers as seen in Fig. 3a and b SEM images of the samples. As the shear bands are well separated both at $\gamma_{pl} = 0.013$ and 0.033 plastic strains, only a few bands intersect the marked area. Fig. 3a exhibits a single straight shear band aligned to $\phi = 84.5$ deg to the torsion axis in the $\gamma_{pl} = 0.013$ sample. At the intersection of the band and the marker line, the offset of the shear band ($\Delta = 3$ μm) after a load-unload cycle can be determined accurately from the shift of the marker line. When torsion shear strain is increased up to $\gamma_{pl} = 0.033$, the morphology of the shear pattern undergoes drastic change (see Fig. 3b). Two bands exhibit distinct and straight shear trajectories aligned to $\phi_A = 83.0$ deg (shear band A) and $\phi_B = 10.4$ deg (shear band B) to the rotational axis. In torsion deformation, locally, the stress field can be approximated by a single shear component, therefore shear planes mirrored to the $\phi = 45$ deg direction are equivalent which explains the appearance of the two kinds of SBs. Delayed appearance of the bands parallel to shear band B infers that SB formation is a non-local, cooperative process which is sensitive to the global asymmetry, i.e. the geometry of the sample.

The off aligned SBs in Fig. 3b intersect each other and exhibit an interaction (see the area indicated by dotted red line). Interestingly, asymmetry was observed in different characteristics between the two intersecting bands. While, the offset of shear band A is practically constant ($\Delta_A = 7.35$ μm), the offset of shear band B varied in the $\Delta_B = 2.3$–2.6 μm range. (Here, offsets of the shear bands are also determined from their intersections with different marker lines, of which only the nearest ones to the interaction area are shown in Fig. 3b). In addition to the markers, fine polishing scratches can also be applied systematically to determine the band offsets distribution of shear band B quantitatively. The obtained $\Delta_B(x)$ offset distribution as a function of the distance from the position of the intersection of the bands (x) are plotted in Fig. 4. As one can notice, $\Delta_B(x)$ increases progressively from $\Delta_B(0) = 1.78$ μm close to the intersection of the bands and reaches the maximum ($\Delta_B(a) = \Delta_B(0) +$

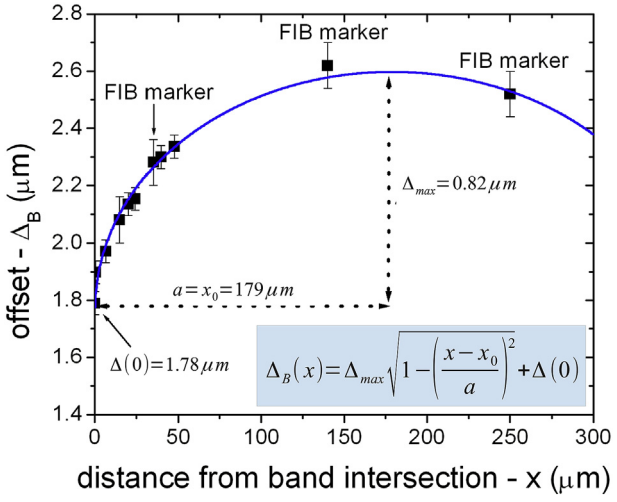

Fig. 4. (a) Enlarged view of the band intersection area shown in Fig. 3b. (b) Reconstructed offsets of the numbered events for shear band B as a function of the offsets in shear band A.

$\Delta_{max} \approx 2.6$ μm) at a distance a ≈ 180 μm. (The continuous blue line is a fit of the function indicated in Fig. 4.). This progressive change of $\Delta_B(x)$, which follows a square root behavior near the intersection area, is typical for sheared planar faults. Therefore, it indicates the presence of a stress concentration which can be characterized by a $K_{II} = \Delta_{max}\kappa\sqrt{\pi/a} = 2.79 MPa\sqrt{m}$ stress intensity factor [27], where $\kappa = 0.5G/(1-\nu)$, $G = 33.2$ GPa is the shear modulus and $\nu = 0.36$ is the Poisson number of the metallic glass [28,29].

Additionally, the shear band intersection exhibit other asymmetric features in Fig. 3b. In spite of the continuous deformation, shear band B splits into a few discrete shear bands due to the band interaction. While shear band A keeps its original straight direction without any splitting. Close up view of the SB intersection area shown in Fig. 5a reveals fine details of the interaction, namely, shear band A breaks into zigzag-like segments at positions where the new trajectories of shear band B stem from. Relative positions of a band segments with respect to the original position of the corresponding band (as determined by the markers) allows to reconstruct the history of successive shear offsets during the torsion process (see Fig. 5a). Fig. 5b depicts Δ_B as a function of Δ_A in this selected SB intersection area describing quantitatively the

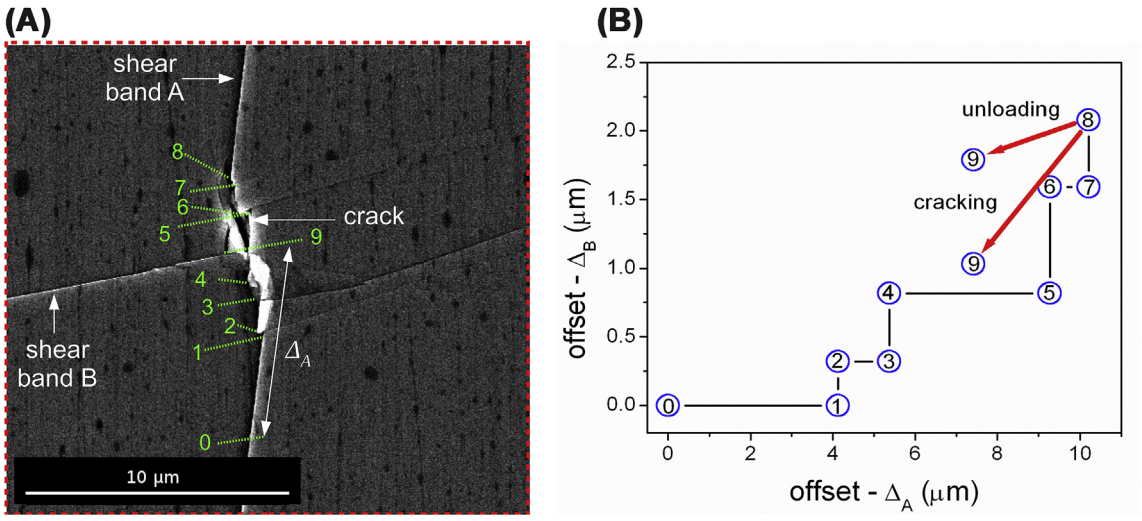

Fig. 5. Offset distribution along shear band B as a function of distance from the band intersection with a fit analytical curve.

evolution of discrete shear band slips. The segments of the individual slip events in Fig. 5a and the corresponding offsets in Fig. 5b are denoted by the same number. The first slip event of shear band B took place only after $\Delta_A = 4.1$ μm offset of the shear band A in agreement to the observed (single slip) shear bands in Fig. 3a. The last slip events (event 8 and 9) indicate a reverse slip (i.e. relaxation) and local fracture of the sample.

In general, SB trajectories exhibit offsets also in radial direction (otherwise SEM would not image band trajectories). These radial offsets were revealed by AFM scans on the surface of the deformed samples. Fig. 6a presents the topography map after the removal of the sample curvature in an AFM scan at the same band intersection area as shown Fig. 3b. The radial offsets along the shear bands are approximately constant, i.e. 150 nm ± 10 nm for SB A and 50 nm ± 10 nm for SB B. Fig. 6b plots the height variation parallel to SB B close to the upper and lower edges of the band. As seen, profile 1 exhibits only the radial offset of SB A, while profile 2 shows a well defined material pile-up observed at the band intersection point with vertical offset reaching 300–400 nm.

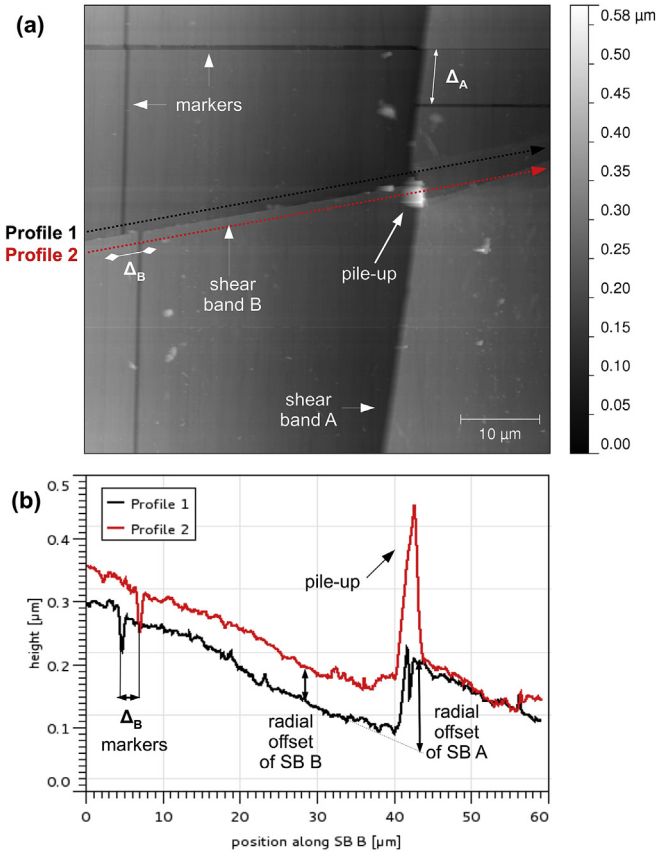

Fig. 6. (a) AFM map shows the radial surface displacements of the same area as shown in Fig. 3b.
(b) Surface height profiles along the lower (Profile 1) and the upper (Profile 2) edges of SB B.

4. Simulation

In order to interpret the formation of stress concentrations around intersecting bands and reveal the reason of the observed asymmetry, a linear continuum shear band model was constructed in the following way. Band trajectories were divided into segments and the stress field of each segment was approximated by that of a pair of line defects enclosing the local Δ offset of the shear band segment (see Fig. 7). In the pair, each line defect was straight and had equal size but with opposite sign. Although, the elemental displacements are the highly localized STZs in the glassy structure, for the sake of simplicity we applied elemental displacements with linear shape and infinite length in the present calculations. Specifically, the shear bands were straight in the x-y plane and infinite in the perpendicular z direction (see Fig. 7). Due to the similar geometrical features, the line defects in the dipoles (similarly to edge dislocations in crystalline materials) were denoted by $\perp$ and $\top$ and had a $\sigma_{xy} = \alpha x(x^2 - y^2)/(x^2 + y^2)^2$ shear stress field component based on the elastic continuum expression valid for macroscopic samples [30], where $\alpha = G\Delta/[2\pi(1-\nu)]$.

Taking into account the malleability of the shear bands, the local offset was varied in a self consistent way in each segment by limiting the shear stress to τ_{SB}, the strength of the band and applying no resistance against shearing when shear stress exceeds, $|\sigma_{xy}| > \tau_{SB}$. Therefore, elemental displacements were formed along segments of the band trajectory until the shear offset reached an equilibrium Δ(x) value at which the magnitude of the local shear stress drops below τ_{SB}. Local stress was calculated as a sum of the stress field of the band segments and the external shear stress field

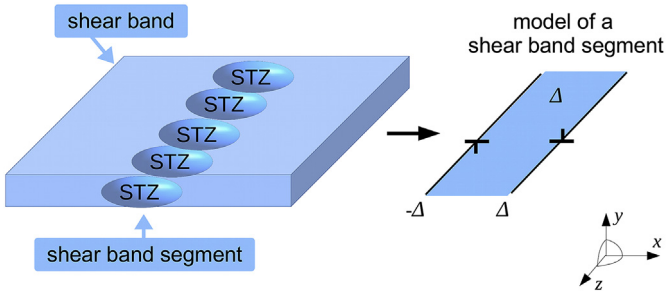

Fig. 7. Schematic image of a thin shear band segment with Δ offset in the x-z plane consists of a line of STZs and its stress field model composed of a dipole of line defects.

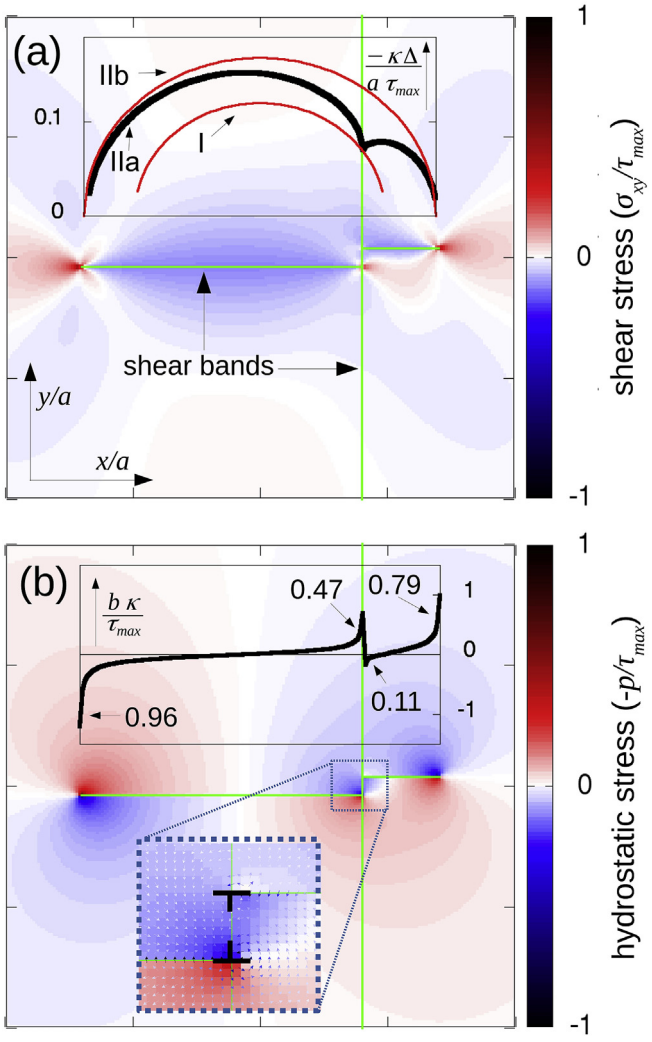

Fig. 8. (a) Simulated residual shear stress around two intersecting shear bands (band trajectories are indicated by green color). The upper inset shows the offset distribution of the horizontal band before intersection with the vertical band (curve I) and the offset distributions of the elongated horizontal band with (curve IIa) and without (curve IIb) band intersection. (b) Hydrostatic stress component of the intersecting bands. It concentrates at the ends of the band in coincidence to the derivative of the offset distribution (upper inset). Ratio of the stress intensity factors of the IIa curve and that of the reference IIb curve is shown at the band ends in the upper inset. The lower inset is an enlarge region of the band intersection area with schematic line defects indicating the high number of opposite sign line defects accumulated at the band ends. (For interpretation of the references to color in this figure legend, the reader is referred to the Web version of this article.)

(τ_{ext}). Shape and length of the shear band were kept constant during the stress calculation. Although, the applied glass model omits the strongly deformation dependent viscosity of the material, it significantly simplifies the calculations and helps to focus on the stress field related features of the shear bands. For further details on the model simulations see the Appendix.

5. Discussion

Model simulations for a simple straight shear band with $\tau_{SB} = 0$ reproduced correctly (not shown here) the external stress dependent reversible $\Delta(a, \tau_{ext}) = \Delta_{max}\sqrt{1-(x/a)^2}$ analytical offset distribution of the equivalent mode II crack, with $\Delta_{max} = a\tau_{ext}/\kappa$. By comparing this Δ_{max} quantitatively to the experimental results obtained for shear band B, the calculated $\Delta_{max}/a = 4.58 \cdot 10^{-3}$value deviates from $\tau_{ext}/\kappa = 3.85 \cdot 10^{-2}$determined for Vitreloy1b, where $\tau_{ext} = \tau_{max} = 1GPa$was taken the maximum of the shear stress (see Fig. 2b). Since the reduction of the shear stress along the band is proportional to the magnitude of the offset (Δ_{max}), the difference between the two values indicates, that SB B should exhibit a finite strength for which an upper limit can be calculated, $0 < \tau_{SB} < 1-(\Delta_{max}\kappa/a) \approx 0.88\tau_{\max}$. In agreement with the measured offset distribution (see Fig. 4), at finite strength, SBs can withstand shear stress changes during unloading and, therefore, the stress field formed around a band at maximum load is preserved.

This residual stress field is also reconstructed in a simulation for two intersecting SBs. Fig. 8a depicts the shear (σ_{xy}) and Fig. 8b the hydrostatic ($-p = (\sigma_{xx} + \sigma_{yy} + \sigma_{zz})/3$) components of the residual stress field for the intersecting SBs. Here, similarly to the shear stress, the hydrostatic stress field was calculated as the sum of the hydrostatic stress components of line defects [30]. In the simulations, consecutive steps of band lengthening for a horizontal and a vertical bands were applied alternately at constant $\tau_{ext} = \tau_{max}$ to produce a shear band evolution revealed in Fig. 5b (for details see the Appendix). As seen in Fig. 8a, the shear stress is concentrated at the tips of the bands, while a $\tau_{SB}-\tau_{\max}$ back stress develops along the trajectory of the shear band. The inset shows the offset distribution of the horizontal band before intersection with the vertical band (curve I) and the offset distributions of the lengthened horizontal band with (curve IIa) and without (curve IIb) band intersection. For straight bands without band intersection the offset follows $\Delta(x) = a\sqrt{1-(x/a)^2}(\tau_{max}-\tau_{SB})/\kappa + \Delta_0$ with $\Delta_0 = 0$, while similar approximate expressions with $\Delta_0 \neq 0$ fit well to the left and right part of the displaced band. Due to the lengthening of the shifted horizontal band parts, STZs (i.e. dipoles of line defects in the present simulation) form at all band segments and increase the Δ offset except at the ends of the bands (cf. curves I and IIa in the inset of Fig. 8a). In parallel, as one can notice, the line defects accumulate at the ends of the bands and the derivative of the offset ($b(x) = \frac{\partial\Delta(x)}{\partial x}$) becomes divergent also at the new tips of the horizontal band with non-zero stress intensity factor (see the upper inset of Fig. 8b). Ratio of the stress intensity factors of the IIa curve and that of the reference IIb curves (indicated in the upper inset of Fig. 8b) shows that band intersection reduces the stress concentration for each tip of the band and leads different stress intensity factors for the new band ends (e.g. 0.11 for the right hand side of the upper segment and 0.47 for the left hand side of the lower segment). We presume, that the formed stress intensity factors are responsible for the subsequent growth of the displaced bands. Therefore, qualitatively, this behavior predicts an asymmetry in band formation, i.e. it explains why SB B extends asymmetrically only to the right from the band intersection as observed in Figs. 3b and 5a.

The other striking feature of Fig. 3b, namely that SB A follows a single trajectory, raises an important question: How can SB A produce Δ offsets uniformly also along those band segments which are

parallel to SB B? We answer this question based on the hydrostatic stress component which has a key role in the plastic deformation of glasses [31]. Fig. 8b exhibits the hydrostatic stress field around the intersecting shear bands. As seen, it is proportional to $b(x)$along the band, but with opposite sign at the sides of the band and it is accompanied also with severe stress concentrations at the tips of the bands. If the displaced band segments of SB A operate as individual bands, the divergence of b should have opposite signs similarly to the horizontal band in Fig. 8b. Upon loading, this special polarized divergent line fault distribution – which is in fact geometrically necessary – always induces compressive stress and density increase in the volume between the two displaced band segments (see the lower inset of Fig. 8b in which we indicated the opposite sign of the line defects by $\perp$ and $\top$). In order to get uniform $\Delta(x)$ along the displaced band segments of shear band A, the line defects with opposite divergence should be eliminated; however, this process requires long range atomic redistribution, the diffusion of atoms which are responsible for the density increase in the volume between the two SB tips. Primarily, these extra atoms induce volumetric distortion (they are dilatational defects) in the glassy matrix, therefore a netforce acts on them in the direction of gradients of the hydrostatic stresses. Since, long range atomic diffusion slows down below the glass transition temperature in metallic glasses, the role of large stress gradients is essential in this diffusion process. However, atomic mobility in shear bands surpass that of the bulk glass by several orders of magnitude [32], therefore the intersecting shear band not only displace the other band, but it may take place in the removal of extra atoms in between the two displaced ends of the other band. This process leads to a "communication" between the displaced ends of the shear band, so that displaced bands can be regarded as a single shear band as long as the offset is not too large to remove the extra atoms by diffusion. Furthermore, the process also reveals that, how intersecting shear bands preserve their discrete behavior when they interact with each other in metallic glasses.

6. Summary

Intersecting shear bands were observed in Vitreloy1b bulk metallic glass subjected to room temperature plastic deformation in torsion. In spite of the continuous deformation, the bands split into discrete band segments and exhibited band interaction which was asymmetric regarding the two bands. Shear offset distributions along the bands were measured in an area defined by focused ion beam milled markers and severe concentration of the residual stress was evidenced. Asymmetry of the band interaction and different characteristics of the residual stress field around the shear bands were reproduced in a simulations based on dipoles of immobile line faults. Comparison of the experimental and the simulation results revealed a diffusion process of dilatational defects which takes place in shear band interaction.

Declaration of competing interest

The authors declare that they have no known competing financial interests or personal relationships that could have appeared to influence the work reported in this paper.

Acknowledgements

This work was completed in the ELTE Institutional Excellence Program (1783–3/2018/FEKUTSRAT) supported by the Hungarian Ministry of Human Capacities. The authors are indebted for V.K. Kis for valuable discussions and G. Varga for SEM experiments.

Appendix

Simulations were performed with different parameters and band arrangements in this work. This is described in detail as follows.

1) Initially in a simple shear band geometry (straight SB with $2a$ length consisting of 100 line segments) was applied with $\tau_{SB} = 0$ shear band strength and different stress field components were determined at an τ_{ext} external stress field. This configuration leaded to a reversible stress field around the shear band with varying external stress.
2) In a second step, the same simulation with $\tau_{SB} \neq 0$was used loading the band to $\tau_{ext} = \tau_{max}$external stress and then unloading it to zero external stress. After this simulation, an irreversible component of the stress field is found, and after unloading a residual stress field is preserved.
3) In a third simulation step, the residual stress field around two intersecting shear bands was determined. Basically, band intersection is due to a crossing band in which the local offset increases. As the offset distribution depends primarily on the length of the band (and also on the maximum of the external stress which was approximately constant in the present test as seen in Fig. 2b), hereby, band intersections were simulated by increasing the band length of a crossing bands. Therefore, in the simulation the following steps were performed. i) A straight, "horizontal" band was formed with $2a$ length consisting of 100 line segments in the x direction. ii) The external stress was increased to $\tau_{ext} = \tau_{\max}$ and the shear band strength was kept constant in the "horizontal" band ($\tau_{SB} = 0.88\tau_{\max}$). iii) A straight, "vertical" band was formed in the y direction, which intersected the "horizontal" band at 0.7a and induced a $\Delta_{\text{vertical}} = 0.16a$ offset. For the sake of simplicity, the "vertical" band had infinite length and produced constant Δ_{vertical} offset along it length having no contribution to the stress field. iv) The two displaced parts of the "horizontal" band extended by producing a $0.4a$ length increase at the original ends of the band. v) The intersecting shear bands were unloaded to $\tau_{ext} = 0$. Here, the contributions to the stress field were also neglected from the "vertical" band.

Author statements

Zsolt Kovács: conceptualization, planning the experiments, investigations, software preparation, visualization of the data, writing draft and reviewing the manuscript.

Ádám Révész: investigations, writing and reviewing of the manuscript.

Mohammed Ezzeldien: planning the experiments, investigations.

János Lendvai: conceptualization, writing and editing of the manuscript, funding acquisition.

References

[1] P. Duwez, R.H. Willen, W. Klement, Continuous series of metastable solid solutions in silver-copper alloys, J. Appl. Phys. 31 (1960) 1136–1137.
[2] C.J. Gilbert, R.O. Ritchie, W.L. Johnson, Fracture toughness and fatigue-crack propagation in a Zr–Ti–Ni–Cu–Be bulk metallic glass, Appl. Phys. Lett. 71 (1997) 476–478.
[3] J. Xu, U. Ramamurty, E. Ma, The fracture toughness of bulk metallic glasses, J. Occup. Med. 62 (2010) 10–18.
[4] A.L. Greer, Metallic glasses, Science 267 (1995) 1947–1953.
[5] A. Inoue, Stabilization of metallic supercooled liquid and bulk amorphous alloys, Acta Mater. 48 (2000) 279–306.
[6] C.A. Schuh, T.C. Hufnagel, U. Ramamurthy, Mechanical behavior of amorphous

alloys, Acta Mater. 55 (2007) 4067–4109.
[7] A.L. Greer, Y.Q. Cheng, E. Ma, Shear bands in metallic glasses, Mater. Sci. Eng. R 74 (2013) 71–132.
[8] E.R. Homer, Examining the initial stages of shear localization in amorphous metals, Acta Mater. 63 (2014) 44–53.
[9] Z.Y. Liu, Y. Yang, C.T. Liu, Yielding and shear banding of metallic glasses, Acta Mater. 61 (2013) 5928–5936.
[10] H.S. Shahabi, S. Scudino, I. Kaban, M. Stoica, U. Rütt, J. Eckert, Structural aspects of elasto-plastic deformation of a Zr-based bulk metallic glass under uniaxial compression, Acta Mater. 95 (2015) 30–36.
[11] S. Feng, L. Qi, L. Wang, S. Pan, M. Ma, X. Zhang, G. Li, R. Liu, Atomic structure of shear bands in $Cu_{64}Zr_{36}$ metallic glasses studied by molecular dynamics simulations, Acta Mater. 95 (2015) 236–243.
[12] C.A. Pampillo, Localized shear deformation in a glassy metal, Scr. Metall. 6 (1972) 915–918.
[13] Y. Zhang, A.L. Greer, Thickness of shear bands in metallic glasses, Appl. Phys. Lett. 89 (2006), 071907.
[14] A.S. Argon, Plastic deformation in metallic glasses, Acta Metall. 27 (1979) 47–58.
[15] E. Ma, Tuning order in disorder, Nat. Mater. 14 (2015) 547–552.
[16] D. Klaumünzer, R. Maaß, J.F. Löffler, Stick-slip dynamics and recent insights into shear banding in metallic glasses, J. Mater. Res. 26 (2011) 1453–1463.
[17] R.T. Qu, H.S. Liu, Z.F. Zhang, In situ observation of bending stress–deflection response of metallic glass, Mater. Sci. Eng. A 582 (2013) 155–161.
[18] Zs Kovács, L.S. Tóth, J. Lendvai, Ideal elasto-plastic behavior in torsional deformation of $Zr_{44}Ti_{11}Cu_{10}Ni_{10}Be_{25}$ bulk metallic glass, J. Alloy. Comp. 542 (2012) 85–89.
[19] M. Ezzeldien, Zs Kovács, J. Lendvai, F. Chmelík, K. Máthis, Stages in room temperature torsional deformation of a Vitreloy bulk metallic glass, J. Alloy. Comp. 577 (2013) 25–29.
[20] J. Li, Z.L. Wang, T.C. Hufnagel, Characterization of nanometer-scale defects in metallic glasses by quantitative high-resolution transmission electron microscopy, Phys. Rev. B 65 (2002), 144201.
[21] R. Maas, P. Birckigt, C. Borchers, K. Samwer, C.A. Volkert, Long range stress fields and cavitation along a shear band in a metallic glass: the local origin of fracture, Acta Mater. 98 (2015) 94–102.
[22] H.S. Shahabi, S. Scudino, I. Kaban, M. Stoica, B. Escher, S. Menzel, G.B.M. Vaughan, U. Kühn, J. Eckert, Mapping of residual strains around a shear band in bulk metallic glass by nanobeam X-ray diffraction, Acta Mater. 111 (2016) 187–193.
[23] A. Vinogradov, M. Seleznev, I.S. Yasnikov, Dislocation characteristics of shear bands in metallic glasses, Scr. Mater. 130 (2017) 138–142.
[24] M. Hafok, R. Pippan, Post-shear deformation of high pressure torsion-deformed nickel under hydrostatic pressure, Scr. Mater. 56 (2007) 757.
[25] Zs Kovács, E. Schafler, P. Szommer, Á. Révész, Localization of plastic deformation along shear bands in Vitreloy bulk metallic glass during high pressure torsion, J. Alloy. Comp. 593 (2014) 207–212.
[26] Á. Révész, Zs Kovács, Severe plastic deformation of amorphous alloys, JIMM Materials Transactions 60 (2019) 1283–1293.
[27] C.T. Sun, Z.H. Jin, Fracture Mechanics, Elsevier Inc., 2012.
[28] W.L. Johnson, M.D. Demetriou, J.S. Harmon, M.L. Lind, K. Samwer, Rheology andultrasonic properties of metallic glass-forming liquids: a potential energy landscape perspective, MRS Bull. 32 (2007) 644–650.
[29] J.C. Li, X.W. Chen, F.L. Huang, Inhomogeneous deformation in bulk metallic glasses: FEM analysis, Mater. Sci. Eng. A 620 (2015) 333–351.
[30] I. Kovács, L. Zsoldos, Dislocations and Plastic Deformation, Akadémia Kiadó, 1973.
[31] J. Pan, Y.X. Wang, Q. Guo, D. Zhang, A.L. Greer, Y. Li, Extreme rejuvenation and softening in bulk metallic glass, Nat. Commun. 9 (2018) 1–9.
[32] J. Bokeloh, S.V. Divinski, G. Reglitz, G. Wilde, Tracer measurements of atomic diffusion inside shear bands of a bulk metallic glass, Phys. Rev. Lett. 107 (2011), 235503.